


Diffusion in Mesoscopic Lattice Models of Amorphous Plasticity

Botond Tyukodi,^{1,2,3} Damien Vandembroucq,¹ and Craig E Maloney²

¹*PMMH, ESPCI Paris, CNRS UMR 7636, Sorbonne Université, Université Paris Diderot, PSL Research University 10 rue Vauquelin, 75231 Paris cedex 05, France*

²*Department of Mechanical and Industrial Engineering, Northeastern University, Boston, Massachusetts 02115, USA*

³*Department of Physics, Babeş–Bolyai University, Cluj-Napoca 400084, Romania*

 (Received 15 March 2018; revised manuscript received 21 May 2018; published 1 October 2018)

We present results on tagged particle diffusion in a mesoscale lattice model for sheared amorphous material in athermal quasistatic conditions. We find a short time diffusive regime and a long time diffusive regime whose diffusion coefficients depend on system size in dramatically different ways. At short time, we find that the diffusion coefficient, D , scales roughly linearly with system length, $D \sim L^{1.05}$. This short time behavior is consistent with particle-based simulations. The long-time diffusion coefficient scales like $D \sim L^{1.6}$, close to previous studies which found $D \sim L^{1.5}$. Furthermore, we show that the near-field details of the interaction kernel do not affect the short time behavior but qualitatively and dramatically affect the long time behavior, potentially causing a saturation of the mean-squared displacement at long times. Our finding of a $D \sim L^{1.05}$ short time scaling resolves a long standing puzzle about the disagreement between the diffusion coefficient measured in particle-based models and mesoscale lattice models of amorphous plasticity.

DOI: [10.1103/PhysRevLett.121.145501](https://doi.org/10.1103/PhysRevLett.121.145501)

Many systems in condensed matter physics [1], including pinned contact lines [2,3], charge density waves [4], dislocations in crystals [5–7], disordered magnets [8], and others exhibit bursty, intermittent relaxation during avalanches when slowly driven. One may ask how the avalanches give rise to spatial correlations of activity on longer times corresponding to the operation of many successive individual avalanches. For instance, for the case of pinned lines, the geometry of the front evolves according to the Family-Vicsek scaling laws [9], and it is natural to ask whether similar scaling laws govern long-time patterns of activity in related avalanching systems. In this Letter, we study these long-time correlations in a mesoscale model for a sheared amorphous solid. Many different materials can exist as amorphous solids. Examples include amorphous metallic alloys [10], emulsions [11,12], microgel suspensions [13], confined granular packings [14], etc.

Over the past few decades, the notion of local shear transformations has been used to describe and explain the plastic flow of amorphous solids [15,16]. A class of mesoscopic lattice models is built on this picture [17–29], (see Nicolas *et al.* [30] for a recent review). In these lattice models, the system is partitioned into local regions, and any one of them may undergo a yielding event if loaded beyond some threshold. These models are designed to operate at a mesoscopic scale, slightly coarser than the particles, but not at a macroscopic scale where continuum thermodynamic models describe phenomena such as persistent shear localization [16,31,32].

Avalanches of local shear transformations are observed in both particle-scale [33–36] and mesoscale models [19,20,28,29,37,38] during slow steady shear. The cascades are caused by the elastically mediated redistribution of stress after a local yielding event [15,21,39]. The result is a broad spectrum of bursts of plastic activity [10] and fractal patterns of accumulated plasticity [40]. Similar avalanching behavior is observed in many different dynamically critical systems [41–46].

Despite the quantitative agreement in the spectrum of avalanche sizes and the qualitative agreement in the spatial correlations in the plastic strain [18], one major discrepancy between particulate and mesoscale models has remained. It involves the diffusion coefficient, D , of the motion of tagged particles. Lemaître and Caroli [47] argued that the spatial correlations in the plastic strain field should give rise to a dependence of D on the system length, L . In quasistatic simulations of a Lennard-Jones glass, Maloney and Robbins [48] showed that $D \sim L$. In a lattice model, Martens *et al.* [22], found a very different scaling, $D \sim L^{1.5}$. Nicolas and co-workers [24] then showed that including the effects of advection changes the $D \sim L^{1.5}$ scaling and suggested including advection was necessary to obtain agreement with particulate models. However, very little quantitative reconciliation has been done between the mesoscale and particulate models even for this case of advection.

To shed light on these inconsistencies, we have performed an extensive set of simulations of a simple athermal quasistatic mesoscopic lattice model. We find a short time

regime where $D \sim L^{1.05}$, and a long time regime where $D \sim L^{1.6}$. The short time diffusive plateau ends after a characteristic time $\Delta\gamma_* \sim L^{-1.05}$, characterizing the strain released in a system spanning event, which shrinks with system size. This reconciles the $D \sim L^1$ results of reference [48] with the $D \sim L^{1.5}$ results of Refs. [22,24]. The crossover to the long time $D \sim L^{1.6}$ regime occurs at a size independent strain of order unity. Further, we show that the kurtosis of the displacement distribution decays with the size of the time window in the same way as in atomistic simulations and argue that this is a generic consequence of the fact that the displacement field is built from temporally uncorrelated shot noise with the spatial structure of each shot being a characteristic system spanning avalanche.

The basic approach of the lattice models goes back to Eshelby who showed that the linear elasticity problem in which a local region undergoes a shift, ϵ^p , in its reference, stress-free configuration, is given by an integral convolution: $\sigma_{\alpha\beta}(\mathbf{r}) = \int K_{\alpha\beta\mu\nu}^e(\mathbf{r} - \mathbf{r}') \epsilon_{\mu\nu}^p(\mathbf{r}') d\mathbf{r}'$ where K^e is the so-called Eshelby kernel. Lattice models of amorphous plasticity then add a dynamical rule for the evolution of ϵ_p . One of our goals in this study was to develop a simple discretization of the Eshelby problem on a lattice which gives realistic displacements and compatible strains near the lattice site undergoing plasticity. Our approach is detailed in the Supplemental Material [49], but briefly: (i) we define our lattice model by partitioning space into square domains; (ii) we define the strain on each square via a finite difference of a displacement field defined on the vertices of the square, and (iii) the response, σ , to an increment of ϵ^p on a single square—i.e., the Eshelby kernel—is expressed analytically as a Fourier series on the square lattice and tabulated in real space for each lattice size, L . This discretization scheme is similar to that used in studies of Martensitic transformations [50,51] and to a scheme used recently in an amorphous lattice model by Nicolas [52]. At long distances, the shear component of this kernel gives the far-field solution of the Eshelby inclusion problem [39], and its shear component features a quadrupolar symmetry, i.e., in polar coordinates $K_{xyxy}^e(r, \theta) \propto \cos(4\theta)/r^2$.

In this Letter, we focus on two modes of shear with respect to the underlying lattice, $\epsilon_{xx} = -\epsilon_{yy} = \epsilon$, $\epsilon_{xy} = \epsilon_{yx} = 0$ which we call mode 2 and $\epsilon_{xy} = \epsilon_{yx} = \epsilon$, $\epsilon_{xx} = \epsilon_{yy} = 0$ which we call mode 3. We assume the elastic constants have the Lamé form so that, in either case, $\sigma = 2\mu\epsilon^e$, where ϵ^e is the elastic strain. We work in units where $2\mu = 1$ so that we can speak interchangeably of σ or ϵ^e . Denoting spatial averages with $\langle \cdot \rangle$, $\langle \sigma \rangle$, and $\langle \sigma/2\mu + \epsilon^p \rangle$ would be the stress and strain of the sample measured by a load cell. As we will show below, despite residual correlations at long time in mode 2, the short time behavior of modes 2 and 3 in terms of the displacement and strain statistics and the avalanche spectrum (not studied here) is, essentially, indistinguishable.

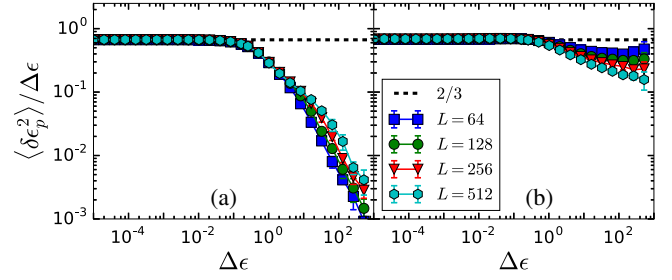


FIG. 1. Variance, $\langle \delta\epsilon_p^2 \rangle$, of the plastic strain field for a given interval of applied strain, $\Delta\epsilon$, scaled by $\Delta\epsilon$ for various system length, L , in (a) mode 2 and (b) mode 3 loading.

We have studied different flavors of the model, characterized by different ways of introducing disorder and advancing the simulation in time. For the stochastic ingredients, we have studied (i) random local stress thresholds, σ_y , with uniform increments in local plastic strain, ϵ^p , and (ii) random increments in ϵ^p with uniform σ_y . For the dynamical rule, we have used (i) an extremal protocol, where the total strain $\epsilon^t = \epsilon^e + \epsilon^p$ is adjusted uniformly across the system at each step so that precisely one site is at threshold [17], and (ii) a synchronous protocol where all unstable sites are updated simultaneously while $\langle \epsilon^t \rangle$ is held fixed, and this procedure is iterated at the same $\langle \epsilon^t \rangle$ until all sites become stable before ϵ^t is incremented again. We have checked that the scaling exponents we define below do not depend on either the stochastic model or dynamical update rule, although nonuniversal properties may. The data we present here are for the case of random ϵ_p increments with uniform σ_y and for the synchronous update protocol. We choose each local increment of ϵ_p from a uniform distribution from 0 to ϵ_0 ($\epsilon_0 = 1$). ϵ_0 is then the only nontrivial adjustable parameter in the model [18,53].

In Figs. 1(a) and 1(b), we show the steady-state variance, $\langle \delta\epsilon_p^2 \rangle$, of the plastic strain field scaled by the length of the time window, $\Delta\epsilon$, as a function of $\Delta\epsilon$ for various system lengths, L , in mode 2 (a) and mode 3 (b) loading. For short times (small $\Delta\epsilon$), both modes of loading show a consistent, size independent, diffusion constant. We can make an *ab initio* estimate for the height of the plateau by assuming the probability distribution of local plastic strains is simply the uniform distribution corresponding to sites which have yielded precisely once plus a residue at zero corresponding to sites which have not yet yielded. This *ab initio* estimate gives a value of $2/3$ which is in excellent agreement with the measured plateau height. At later times, sites will eventually undergo more than one yielding event, and this estimate will break down.

There is a fall off from the plateau, starting at a strain of order 0.5 (regardless of L) at which point each site has yielded approximately once on average. Beyond this fall from the plateau, the two loading modes show dramatically different behavior. The mode 2 curves all drop sharply.

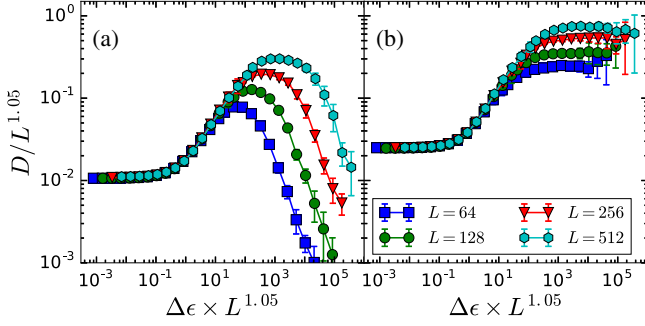


FIG. 2. Diffusion coefficient, $D = \langle \delta \mathbf{u}^2 \rangle / \Delta \epsilon$, of the displacement field scaled by $L^{1.05}$ as a function of $(\Delta \epsilon)L^{1.05}$ for (a) mode 2 and (b) mode 3.

Each curve has a shoulder feature beyond which $\langle \delta \epsilon_p^2 \rangle$ saturates and $\langle \delta \epsilon_p^2 \rangle / \Delta \epsilon \sim 1 / \Delta \epsilon$. The shoulder extends to longer $\Delta \epsilon$ for larger L . In mode 3, after a subdiffusive regime, the curves again approach a diffusive plateau (with a lower diffusion constant than at short time), with the larger systems having a lower long-time diffusion constant. This behavior for mode 2 and mode 3 is consistent with Ref. [20] where it was argued that the presence of null modes in the convolution operator (and associated stress-free slip lines) was necessary for $\langle \delta \epsilon_p^2 \rangle$ to remain diffusive.

In Fig. 2, we show the diffusion coefficient, $D = \langle \delta \mathbf{u}^2 \rangle / \Delta \epsilon$, of the displacement field scaled by $L^{1.05}$ vs $\Delta \epsilon / L^{-1.05}$. This rescaling by $L^{1.05 \pm 0.05}$ collapses the data onto a short-time master curve which has the same shape for both loading modes. For short times, there is a diffusive plateau. As $\Delta \epsilon$ increases, the curve departs upward, superdiffusively, from the plateau. This superdiffusive regime sets in at a characteristic time scale when: $\Delta \epsilon_* / L^{-1.05} \approx 0.5$. To explain the scaling with L , we recall and generalize the arguments of Ref. [48] which were motivated by Ref. [47]. In Fig. 3, we plot the incremental stress field in mode 3 loading for several consecutive nonoverlapping time windows of a size corresponding to the end of the lower plateau in Fig. 2 at the initial stages of the superdiffusive regime. Similar features are observed for the other loading mode but rotated by 45 degrees. The plasticity is organized into line-like features (either vertical or horizontal) which correspond to the directions where K^e is large and positive.

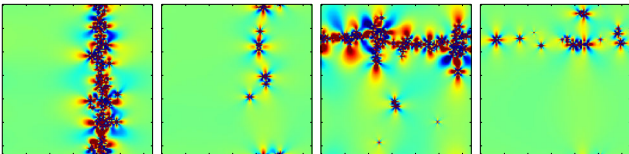


FIG. 3. Mode 3 incremental stress field for several consecutive (nonoverlapping) strain windows of size $\Delta \epsilon = 1 / (2L)$ for $L = 128$ such that, on average, in each window, there are L shear transformations. This corresponds to a $\Delta \epsilon$ for which D has just risen above the lower plateau in Fig. 2.

Suppose the $\Delta \epsilon_p$ field for a typical time window at short time is either zero, if there has been no plasticity, or composed of a perfect line spanning the simulation cell, if there has been plasticity. On average, each site on the line has $\Delta \epsilon_p = \epsilon_0 / 2$. Since there are L/a such sites in the line, the whole line will globally relieve a strain precisely equal to: $\epsilon_s = a \epsilon_0 / 2L$ (where a is the lateral size of a square element of the lattice). The displacement field, \mathbf{u}_s , associated with that slip line is a linear profile with a strain equal to $a \epsilon_0 / 2L$ so that (assuming, for the sake of argument, a horizontal slip line centered at $y = 0$) $u_{sx}(x, y) = 2a(y - L/2)\epsilon_0 / 2L$.

The variance of this displacement field is $\langle \mathbf{u}_s^2 \rangle = a^2 \epsilon_0^2 / 12$ which is independent of L . The rate at which these slip lines occur per unit strain, $N / \Delta \epsilon$, has to be precisely enough so that, on average, $\Delta \langle \epsilon_p \rangle = \Delta \epsilon$ so $N = \Delta \epsilon / \epsilon_s = 2(L/a)(\Delta \epsilon / \epsilon_0)$. If we are in a short time regime so that, at most, one of these slip lines has formed, then we have: $\langle \delta \mathbf{u}^2 \rangle / \Delta \epsilon = N \langle \mathbf{u}_s^2 \rangle / \Delta \epsilon = (L/6)\epsilon_0 a$. So the simpleminded picture of elementary lines predicts a short-time characteristic strain, $\epsilon_s = \epsilon_0 / 2L$ and a short-time $D = (L/6)\epsilon_0 a^2$.

In Fig. 2, we see that the $\epsilon_* \sim L^{-1}$, $D \sim L^1$ scaling is only approximately correct and that scaling ϵ by $L^{-1.05}$ and D by $L^{1.05}$ gives a better quality data collapse for both mode 2 and mode 3 loading. We can explain this by slightly generalizing the argument above. If we imagine the short-time windows contain either no plasticity or a characteristic elementary event, then we still have that $\langle \mathbf{u}^2 \rangle / \Delta \epsilon = N \langle \mathbf{u}_s^2 \rangle / \Delta \epsilon$ where $N / \Delta \epsilon$ is still the rate of events and $\langle \mathbf{u}_s^2 \rangle$ is still the variance of a characteristic event. We still must have balance between applied strain and plastic strain so that $N = \Delta \epsilon / \epsilon_s$, but now ϵ_s is the characteristic strain associated with an arbitrary characteristic event more general than a straight line: $\epsilon_s = n_s (a/L)^2 \epsilon_0 / 2$ where n_s is the number of sites involved in one of the elementary events. For lines, $n_s = (L/a)^1$, while we generalize and let $n_s = A(L/a)^\alpha$ for fractal objects. So for the characteristic strain associated with an elementary line-like object, we have $\epsilon_s = A(L/a)^{\alpha-2} \epsilon_0 / 2$. Finally, for the diffusion, we have $\langle \mathbf{u}^2 \rangle / \Delta \epsilon = 2(L/a)^{2-\alpha} \langle \mathbf{u}_s^2 \rangle / (A \epsilon_0)$. We must assume that the elementary events produce displacement fields whose variance is independent of L , but given that assumption, we see that $D \sim L^{2-\alpha}$ and $\epsilon_s \sim L^{\alpha-2}$. From our scaling collapse, we conclude that $2 - \alpha = 1.05$ which would correspond to a fractal dimension of $\alpha = 0.95 \pm 0.05$.

In Fig. 4, we, again, plot the diffusion coefficient D vs the strain ϵ , but now with D scaled by $L^{1.6}$ to collapse the upper plateau at long time. We see a crossover to the upper plateau at a strain of order unity regardless of L . This occurs after the departure of $\langle \epsilon_p^2 \rangle$ from its short time plateau. The mode 3 case displayed in Fig. 4(b) remains perfectly diffusive for as long as we can simulate, and we

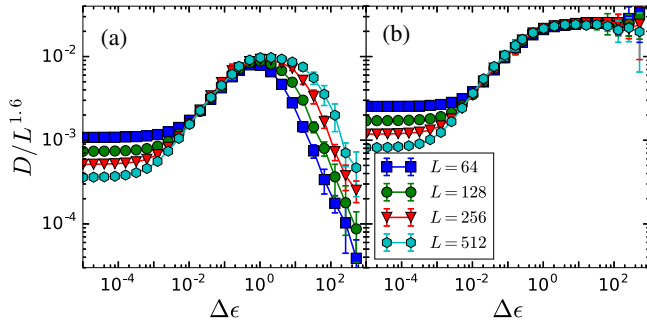


FIG. 4. Diffusivity D scaled by $L^{1.6}$ as a function of $(\Delta\epsilon)$ for (a) Mode 2 and (b) Mode 3.

have no reason to believe it will do otherwise. The mode 2 case shown in Fig. 4(a) shows a strikingly different behavior. For any finite L , the mean square displacement eventually saturates and D decays like $1/\Delta\epsilon$ at long enough $\Delta\epsilon$. Despite this decay, we observe the emergence of an apparent upper plateau before the decay even for mode 2 at sufficiently large L . Furthermore, the height of the plateau seems to obey the $L^{1.6}$ scaling as well. The emergence of the upper plateau in mode 2 appears to be related to the spectral gap in the Eshelby convolution operator disappearing in the $L \rightarrow \infty$ limit [20]. For sufficiently large systems, there will be little difference between mode 2 and mode 3 loading, despite the lack of zero modes of the Eshelby convolution operator in the former, as long as $\Delta\epsilon$ remains below the onset of decay.

In Fig. 5, we plot the kurtosis, K , of the distribution of the u_x (a) and $u_{x45} = (u_x + u_y)/\sqrt{2}$ (b) Cartesian component of the displacement versus $\Delta\epsilon$ for mode 3. Both plots show a striking initial $K \sim 1/\Delta\epsilon$ behavior as observed earlier in Lennard-Jones glasses [54,55]. This can be explained as follows. Suppose the displacement field is built up from a succession of characteristic events which are spatially uncorrelated with each other. Consider a timescale $\Delta\epsilon$ during which it is unlikely to observe more than one event. Then, a typical window of duration $\Delta\epsilon$ contains either one event (with probability $\Delta\epsilon/\epsilon_*$) or no

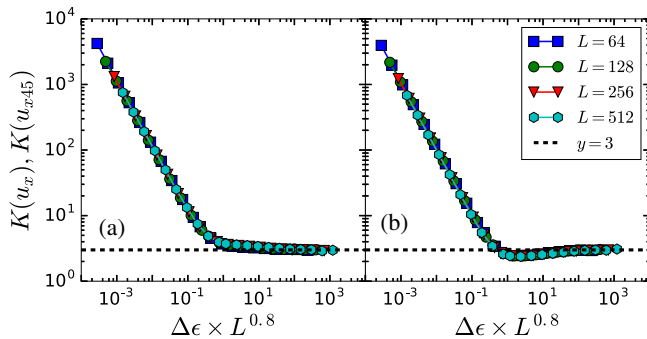


FIG. 5. Kurtosis of the $P(u_x)$ (a) and $P(u_{x45})$ (b) distributions for mode 3. Mode 2 is indistinguishable from mode 3 after interchange of u_{x45} and u_x .

event (with probability $1 - \Delta\epsilon/\epsilon_*$) where ϵ_* is the characteristic strain release in the event. So any particular moment of the distribution should scale like $\langle \delta u^n \rangle \sim \Delta\epsilon$, and, for the kurtosis, $\langle \delta u^4 \rangle / \langle \delta u^2 \rangle^2 \sim \Delta\epsilon / \Delta\epsilon^2 = 1/\Delta\epsilon$ which is precisely what we see and explains the much earlier atomistic results from Tsamados *et al.* [54,55]. At long times, we recover $K \approx 3$, an indication of a Gaussian-like distribution. One might have naively expected the kurtosis data for different system sizes to collapse when $\Delta\epsilon$ is rescaled by the characteristic strain, ϵ_* , which was found above, in the analysis of the diffusion coefficient, to scale like $\epsilon_* \sim L^{1.05}$. However, we find the best collapse for the kurtosis is when $\Delta\epsilon$ is scaled by $L^{0.8 \pm 0.05}$. This discrepancy between the characteristic strain inferred from the diffusion coefficient (the second moment of the displacement distribution) and from the kurtosis (involving both the second and fourth moments) remains an outstanding puzzle.

To summarize, we have shown that lattice models for athermal quasistatic amorphous plasticity show good agreement with particle-based simulations for the system size dependence of the short-time diffusion coefficient. This is for two different stochastic prescriptions for the local energy landscape: random threshold or random plastic strain increment; two different dynamical update rules: synchronous or extremal; and two different orientations of the loading with respect to the lattice. Our results are also in agreement with Maloney and Robbins [48] who showed that the variance of the local strain field shows little size dependence, while the variance of the displacements shows dramatic size dependence.

At longer times, the diffusion coefficient shows a size dependence, $D_e \sim L^{1.6}$ which is extremely close to the $D_e \sim L^{1.5}$ observed in Ref. [22]. In this long time regime, the behavior is different for the two different modes of loading. When loading along the axes of the lattice, the discretized Eshelby kernel has no null modes, so the variance of the plastic strain and, thus, the variance of the displacements, saturates. When loading 45 degrees away, the Eshelby kernel has proper null modes—perfect slip lines along the lattice axes which leave the stress field uniform, so the variance can continue to grow and the system can achieve a proper diffusive limit in agreement with earlier arguments by Tyukodi *et al.* [20]. We note that, even in the axial-load case where there are no perfect null modes of the kernel, a pseudodiffusive plateau develops at the very latest times. The extent of the pseudodiffusive plateau depends on system size with larger sizes maintaining a quasidiffusive regime for a longer period of time, but a precise study of the long-time diffusive behavior is left for future work.

The picture we put forward here of a separate early time diffusive regime crossing over to a distinct late time diffusive regime clarifies the apparent discrepancy between particle-based and lattice-based models. In particular, it appears that the introduction of advection discussed in

Ref. [24] is not necessary to recover the linear size scaling of the correlations observed in atomistic simulations. In light of our present work, it seems likely that a $D_e \sim L^1$ regime was already present in former advection-free lattice models based studies, but that this early diffusive regime was simply not analyzed. Of course, at very late times, advection should be important for a detailed comparison with particle-based simulations.

This material is based upon the work supported by the National Science Foundation under Grant No. NSF/CMMI-1822020 and in part by Grant No. PHY-1748958. C. E. M. would like to acknowledge discussions with Kirsten Martens which motivated this study.

-
- [1] J. P. Sethna, K. A. Dahmen, and C. R. Myers, *Nature (London)* **410**, 242 (2001).
- [2] M. Kardar, *Phys. Rep.* **301**, 85 (1998).
- [3] B. Tyukodi, Y. Bréchet, and Z. Néda, *Phys. Rev. E* **90**, 052404 (2014).
- [4] G. Grüner, *Rev. Mod. Phys.* **60**, 1129 (1988).
- [5] S. Papanikolaou, D. M. Dimiduk, W. Choi, J. P. Sethna, M. D. Uchic, C. F. Woodward, and S. Zapperi, *Nature (London)* **490**, 517 (2012).
- [6] O. U. Salman and L. Truskinovsky, *Phys. Rev. Lett.* **106**, 175503 (2011).
- [7] M.-C. Miguel, A. Vespignani, S. Zapperi, J. Weiss, and J.-R. Grasso, *Nature (London)* **410**, 667 (2001).
- [8] R. C. Buceta and D. Muraca, *Physica (Amsterdam)* **390A**, 4192 (2011).
- [9] H. A. Makse and L. A. N. Amaral, *Europhys. Lett.* **31**, 379 (1995).
- [10] J. Antonaglia, W. J. Wright, X. Gu, R. R. Byer, T. C. Hufnagel, M. LeBlanc, J. T. Uhl, and K. A. Dahmen, *Phys. Rev. Lett.* **112**, 155501 (2014).
- [11] J. Goyon, A. Colin, G. Ovarlez, A. Ajdari, and L. Bocquet, *Nature (London)* **454**, 84 (2008).
- [12] V. V. Vasisht, S. K. Dutta, E. Del Gado, and D. L. Blair, *Phys. Rev. Lett.* **120**, 018001 (2018).
- [13] T. Divoux, C. Barentin, and S. Manneville, *Soft Matter* **7**, 8409 (2011).
- [14] A. Amon, V. B. Nguyen, A. Bruand, J. Crassous, and E. Clément, *Phys. Rev. Lett.* **108**, 135502 (2012).
- [15] V. V. Bulatov and A. S. Argon, *Model. Simul. Mater. Sci. Eng.* **2**, 167 (1994).
- [16] M. L. Falk and J. S. Langer, *Phys. Rev. E* **57**, 7192 (1998).
- [17] J. C. Baret, D. Vandembroucq, and S. Roux, *Phys. Rev. Lett.* **89**, 195506 (2002).
- [18] M. Talamali, V. Petäjä, D. Vandembroucq, and S. Roux, *C. R. Mec.* **340**, 275 (2012).
- [19] M. Talamali, V. Petaja, D. Vandembroucq, and S. Roux, *Phys. Rev. E* **84**, 016115 (2011).
- [20] B. Tyukodi, S. Patinet, S. Roux, and D. Vandembroucq, *Phys. Rev. E* **93**, 063005 (2016).
- [21] G. Picard, A. Ajdari, F. Lequeux, and L. Bocquet, *Eur. Phys. J. E* **15**, 371 (2004).
- [22] K. Martens, L. Bocquet, and J. L. Barrat, *Phys. Rev. Lett.* **106**, 156001 (2011).
- [23] A. Nicolas and J. L. Barrat, *Faraday Discuss.* **167**, 567 (2013).
- [24] A. Nicolas, K. Martens, L. Bocquet, and J. L. Barrat, *Soft Matter* **10**, 4648 (2014).
- [25] A. Nicolas, K. Martens, and J. L. Barrat, *Europhys. Lett.* **107**, 44003 (2014).
- [26] J. Lin, E. Lerner, A. Rosso, and M. Wyart, *Proc. Natl. Acad. Sci. U.S.A.* **111**, 14382 (2014).
- [27] F. Puosi, J. Rottler, and J. L. Barrat, *Phys. Rev. E* **89**, 042302 (2014).
- [28] Z. Budrikis and S. Zapperi, *Phys. Rev. E* **88**, 062403 (2013).
- [29] Z. Budrikis, D. F. Castellanos, S. Sandfeld, M. Zaiser, and S. Zapperi, *Nat. Commun.* **8**, 15928 (2017).
- [30] A. Nicolas, E. E. Ferrero, K. Martens, and J.-L. Barrat, *arXiv:1708.09194 [Rev. Mod. Phys. (to be published)]*.
- [31] M. L. Manning, J. S. Langer, and J. M. Carlson, *Phys. Rev. E* **76**, 056106 (2007).
- [32] E. Bouchbinder and J. S. Langer, *Phys. Rev. E* **80**, 031132 (2009).
- [33] C. E. Maloney and A. Lemaître, *Phys. Rev. E* **74**, 016118 (2006).
- [34] H. G. E. Hentschel, S. Karmakar, E. Lerner, and I. Procaccia, *Phys. Rev. Lett.* **104**, 025501 (2010).
- [35] K. M. Salerno, C. E. Maloney, and M. O. Robbins, *Phys. Rev. Lett.* **109**, 105703 (2012).
- [36] K. M. Salerno and M. O. Robbins, *Phys. Rev. E* **88**, 062206 (2013).
- [37] J. Lin, A. Saade, E. Lerner, A. Rosso, and M. Wyart, *Europhys. Lett.* **105**, 26003 (2014).
- [38] K. Karimi, E. E. Ferrero, and J. L. Barrat, *Phys. Rev. E* **95**, 013003 (2017).
- [39] J. D. Eshelby, *Proc. R. Soc. A* **241**, 376 (1957).
- [40] B. A. Sun and W. H. Wang, *Appl. Phys. Lett.* **98**, 201902 (2011).
- [41] P. Bak, K. Chen, and M. Creutz, *Nature (London)* **342**, 780 (1989).
- [42] P. Bak, C. Tang, and K. Wiesenfeld, *Phys. Rev. Lett.* **59**, 381 (1987).
- [43] A. Tanguy, M. Gounelle, and S. Roux, *Phys. Rev. E* **58**, 1577 (1998).
- [44] L. Ponson and N. Pindra, *Phys. Rev. E* **95**, 053004 (2017).
- [45] A. Benassi and S. Zapperi, *Phys. Rev. B* **84**, 214441 (2011).
- [46] D. S. Fisher, *Phys. Rep.* **301**, 113 (1998).
- [47] A. Lemaître and C. Caroli, *Phys. Rev. Lett.* **103**, 065501 (2009).
- [48] C. E. Maloney and M. O. Robbins, *J. Phys. Condens. Matter* **20**, 244128 (2008).
- [49] See Supplemental Material at <http://link.aps.org/supplemental/10.1103/PhysRevLett.121.145501> for a detailed description of the discretization of the Eshelby kernel.
- [50] S. Kartha, Ph.D. thesis, Cornell University, 1994.
- [51] S. R. Shenoy, T. Lookman, A. Saxen, and A. R. Bishop, *Phys. Rev. B* **60**, R12537 (1999).
- [52] A. Nicolas, F. Puosi, H. Mizuno, and J. L. Barrat, *J. Mech. Phys. Solids* **78**, 333 (2015).
- [53] Z. Budrikis, D. F. Castellanos, S. Sandfeld, M. Zaiser, and S. Zapperi, *Nat. Commun.* **8**, 15928 (2017).
- [54] M. Tsamados, Ph.D. thesis, Université Claude Bernard, 2009.
- [55] M. Tsamados, A. Tanguy, C. Goldenberg, and J. L. Barrat, *Phys. Rev. E* **80**, 026112 (2009).